A real-time IGRT method using a Kalman filter framework to extract 3D positions from 2D projections

To cite this article before publication: Doan Trang Nguyen *et al* 2021 *Phys. Med. Biol.* in press https://doi.org/10.1088/1361-6560/ac06e3

A real-time IGRT method using a Kalman filter framework to extract 3D positions from 2D projections

Doan Trang Nguyen[1,2], Paul Keall[1], Jeremy Booth[3,4], Chun-Chien Shieh[2], Per Poulsen[5] and Ricky O'Brien[2]

[1] School of Biomedical Engineering, University of Technology Sydney, Sydney, New South Wales, Australia

[2] ACRF Image X Institute, The University of Sydney, Sydney, New South Wales, Australia

[3] Northern Sydney Cancer Care Centre, The Royal North Shore Hospital, St Leonards, New South Wales, Australia

[4] School of Physics, The University of Sydney, Sydney, New South Wales, Australia

[5] Department of Radiation Oncology, Aarhus University Hospital, Aarthus, Denmark

Abstract. Purpose: To estimate 3D prostate motion in real-time during irradiation from 2D prostate positions acquired from a kV imager on a standard linear accelerator utilising a Kalman Filter (KF) framework. The advantage of this novel method is threefold: (1) eliminating the need of an initial learning period, therefore reducing patient imaging dose, (2) more robust against measurement noise and (3) more computationally efficient. In this paper, the novel KF method was evaluated *in silico* using patients' 3D prostate motion and simulated 2D projections.

Methods: A KF framework was implemented to estimate 3D motion from 2D projection measurements in real-time during prostate cancer treatments. The noise covariance matrix was adaptively estimated from the previous 10 measurements. This method did not require an initial learning period as the KF process distribution was initialised using a population covariance matrix. This method was evaluated using a ground-truth motion dataset of 17 prostate cancer patients (536 trajectories) measured with electromagnetic transponders. 3D motion was projected onto a rotating imager (SID=180cm) (pixel size=0.388mm) and rotation speed of $6°/s$ and $2°/s$ to simulate VMAT treatments. Gantry-varying additive random noise ($\leq$ 5 mm) was added to ground-truth measurements to simulate segmentation error and image quality degradation due to the patient's pelvic bones. For comparison, motion was also estimated using the clinically implemented Gaussian Probability Density Function (PDF) method initialised with 600 projections.

Results: Without noise, the 3D root-mean-square-errors (3D RMSEs) of motion estimated by the KF method were 0.4 ± 0.1 mm and 0.3 ± 0.2 mm for $2°/s$ and $6°/s$ gantry rotation, respectively. With noise, 3D RMSEs of KF estimated motion were 1.1 ± 0.1 mm for both slow and fast gantry rotation scenarios. In comparison, using a Gaussian PDF method, with noise, 3D RMSE was 2 ± 0.1 mm for both gantry rotation scenarios.

Conclusion: This work presents a fast and accurate method for real-time 2D to 3D motion estimation using a Kalman filter approach to handle the random-walk component of prostate cancer motion. This method has sub-mm accuracy and is

highly robust against measurement noise.

1. Introduction

In current radiation therapy, image guided radiation therapy (IGRT) is routinely applied at the start of treatment to align the target with its planned position. However, tumours in the thorax, abdomen and pelvis are not static during treatment. Hence, methods to monitor tumour motion during treatment are highly desirable, even more so with dose escalation and hypofractionation.

In the case of prostate cancer radiotherapy treatments, studies with electromagnetic transponders showed that the prostate can travel up to 15 mm during treatment (Langen et al. 2008). As prostate stereotactic body radiotherapy (SBRT) treatments become clinical standard, it is recommended that real-time motion monitoring is used during these high dose treatments to ensure the dose delivered faithfully reflects the treatment plan (Lovelock et al. 2014). A number of different intrafraction real-time guidance methods have been used during prostate cancer treatments. Systems such as CyberKnife (Accuray, Sunnyvale, CA) and the real-time tracking radiotherapy (RTRT) system use real-time kilovoltage (kV) images from two (CyberKnife) or four (RTRT system) orthogonal room-mounted imagers to track the prostate position based on segmented positions of implanted fiducial markers (King et al. 2009, Kitamura et al. 2002, Sazawa et al. 2009, Shimizu et al. 2000, Shirato et al. 2003, 2000)). The commercial systems Calypso (Varian, Palo Alto, CA) (Kupelian et al. 2007) and RayPilot (Micropos, Gothenburg, Sweden) (Castellanos et al. 2012) utilise implanted electromagnetic transponders, transmitting positional signals to an external receiver. Emerging real-time guidance technologies include ultrasonography Ballhausen et al. (2015) and integrated magnetic resonance imaging (MRI)-radiation therapy systems (Fallone et al. 2009, Raaymakers et al. 2009). Common to all these methods is the need for additional dedicated and typically expensive equipment to perform the real-time guidance.

Real-time motion monitoring should ideally be performed using a standard linear accelerator (linac) without relying on additional hardware. To this end, a number of algorithms have been proposed for the purpose of estimating the target's position in 3D based on its location on a 2D image, which can be acquired using a linear accelerator gantry mounted kilovoltage (kV) x-ray imager system. An apparent advantage of utilising the kV imager is that: most modern linear accelerators have a kV imager, mounted orthogonally to the treatment beam. However, as the target position on the kV imager only contains 2D information, a $2D \rightarrow 3D$ target position estimation is often required. The sparse information renders the problem of solving for the target's 3D position ill-posed, hence, some prior knowledge is usually required.

A different approach for $2D \rightarrow 3D$ estimation is to make use of interdimensional correlation (IDC), which works for two reasons: (1) thoracic tumour motion in the anterior–posterior (AP) and left–right (LR) are correlated to its motion in the superior–inferior (SI) direction; and (2) as the gantry rotates around the patient, the SI position of the tumour is always visible on the kV images. Poulsen et al. (2008a)

implicitly incorporated IDC into their Maximum Likelihood Estimation (MLE) of a Gaussian distribution. Other authors have shown that IDC can be used exclusively for 2D-3D estimation, i.e without probability estimation, including (Cho et al. 2012) and (Chung et al. 2016). Unfortunately, for tumours outside of the thoracic and upper abdominal region, the IDC method does not work. Poulsen et al. (2008) proposed a maximum likelihood estimation (MLE) algorithm to estimate the target's 3D position assuming a Gaussian distribution, which can be built after a learning arc. This solution has been clinically implemented as the kilovoltage intrafraction monitoring (KIM) system, and is currently being trialled for real-time tumour motion guidance in a pilot clinical trial and a multi-centre clinical trial (Keall et al. 2016, Nguyen et al. 2017).

Prostate motion represents a particularly challenging problem as the motion is a random walk, with ever fluctuating IDC and motion magnitude (Ballhausen et al. 2015). For accurate estimation of intrafraction prostate motion from 2D projection information, (Poulsen et al. 2009) and subsequent work (Keall et al. 2015) updated the probability density function (PDF) frequently after the initial learning arc of 120 degrees. Such re-optimisation is both time consuming and computationally expensive.

In this work, we present a Kalman filter approach to estimate prostate 3D intrafraction motion from 2D projection information without requiring re-optimisation. Another distinct advantage of our method is that by initialising with a population covariance matrix, a learning period is thus not necessary.

2. Methodology

In this section, we first describe our implementation of a solution for the $2D \rightarrow 3D$ estimation problem using a Kalman filter approach. Then, we present the simulation framework to evaluate our Kalman filter approach in a number of different clinical scenarios using patient prostate traces from a database of 17 patients and 536 treatment fractions (Langen et al. 2008).

2.1. $2D \rightarrow 3D$ prostate motion estimation with a Kalman filter approach

In accordance with Kalman filter literature (Kalman 1960), the following notations are used:

- $\hat{\mathbf{x}}_k$: the estimated positional vector of the target ($\mathbf{x} = [x\ y\ z]^T$ in the patient 3D IEC coordinate system, at the current projection.
- $\hat{\mathbf{x}}_{k-1}$: the estimated positional vector of the target ($\mathbf{x}$) in the previous projection projection.
- $\mathbf{F}_k$: the state transition matrix of the system from $\mathbf{x}_{k-1}$ to $\mathbf{x}_k$.
- $\mathbf{P}_k$: the predicted error covariance matrix at the current projection.
- $\mathbf{Q}_k$: the covariance of the process at the current projection.
- $\mathbf{R}_k$: the covariance of the observation noise at the current projection.

- $\mathbf{z}_k$: the vector of the measurement, i.e. 2D segmentation of the marker, at the current projection, $\mathbf{z}_k = [u_x, u_y]^T$ in the imager coordinate.
- $\widetilde{\mathbf{y}}_k$: the residual error between the estimated measurements and the actual measurements.

In addition, the matrix $\mathbf{H}_k$ denotes the transformation between the target 3D positional vector $\mathbf{x}_k$ and its measurable 2D position on the imager $\mathbf{z}_k = [u_x, u_y]^T$. For a linac geometry, with the imaging system rotates around y–axis, the following projection equation applies:

$$\mathcal{P}(\mathbf{x}_k|\theta) = \begin{pmatrix} u_x \\ u_y \end{pmatrix} = \frac{SID}{SAD - (x\cos\theta + z\sin\theta)}\mathbf{B}(\mathbf{x_k}|\theta) \tag{1}$$

where:

- θ: the current projection angle.
- SID : source to imager distance in mm.
- SAD : source to axis (isocenter) distance in mm.
- $\mathbf{B}(\mathbf{x_k}|\theta) = \begin{pmatrix} x\sin\theta - z\cos\theta \\ y \end{pmatrix}$

While the optimal Kalman filter framework requires $\mathbf{H}_k$ to be linear such that $\mathbf{z}_k = \mathbf{H}_k\mathbf{x}_k$, we approximate $\mathbf{H}_k$ as:

$$\mathbf{H}_k = \frac{SID}{SAD - (\mathbf{x}_{k-1}[1]\cos\theta + \mathbf{x}_{k-1}[3]\sin\theta)}\mathbf{\Theta} \tag{2}$$

with $\mathbf{\Theta} = \begin{pmatrix} cos(\theta) & 0 & sin(\theta) \\ 0 & 1 & 0 \end{pmatrix}$.

Finally, as the prostate generally does not often move or move very little from one projection to the next, the state transition matrix $\mathbf{F}_k$ is initialised and set to the the identity matrix:

$$\mathbf{F} = \mathbf{F}_k = I = \begin{pmatrix} 1 & 0 & 0 \\ 0 & 1 & 0 \\ 0 & 0 & 1 \end{pmatrix} \tag{3}$$

2.1.1. Initialisation Kalman filter is an iterative framework, which allows the optimal estimation of the measurement and process error to be optimally re-estimated from the current and past measurements. To start the iterative process, it is necessary to initialise the following parameters: $\mathbf{Q}_0$, $\mathbf{R}_0$, $\mathbf{P}_0$ and $\mathbf{x}_0$.

As stated above, the matrix $\mathbf{Q}_0$ represents the process covariance, which for the purpose of motion estimation, represents both the range of motion and the

interdimensional correlation of the motion:

$$\mathbf{Q}_k = \Sigma(\mathbf{x}) = \begin{pmatrix} \Sigma(x,x) & \Sigma(x,y) & \Sigma(x,z) \\ \Sigma(y,z) & \Sigma(y,y) & \Sigma(y,z) \\ \Sigma(z,x) & \Sigma(z,y) & \Sigma(z,z) \end{pmatrix} \tag{4}$$

From a large database of 17 prostate motions with 536 motion traces from different treatment days, we obtained the population covariance of prostate motion:

$$\mathbf{Q}_0 = \mathbf{Q}_k = \begin{pmatrix} 0.3136 & 0.0114 & -0.0775 \\ 0.0114 & 1.8820 & 1.5051 \\ -0.0775 & 1.5051 & 2.4733 \end{pmatrix} \tag{5}$$

For the measurement error matrix $\mathbf{R}_0$, initially, it is difficult to estimate the error of the measurement process, we initialised this matrix as:

$$\mathbf{R}_0 = \begin{pmatrix} 0.2 & 0.2 \\ 0.2 & 0.2 \end{pmatrix} \tag{6}$$

with the intention that $\mathbf{R}_k$ will be updated using the measurement history. The value 0.2 was chosen to give reasonable credit to the measurement system initially. As the measurement error matrix will be updated as soon as the measurement, i.e. projection, occured, this initial value is actually not important for our Kalman filter framework. With similar logic, error matrix $\mathbf{P}_0$ is also initialised to be a zero matrix with the reasonable expectation that the entire system has limited to no error.

Finally, $\mathbf{x}_0$ was initialised to the initial prostate position of the patient on the treatment day. In a realistic clinical scenario, a patient's markers would be the used. The initial markers' position of the day can be easily obtained by performing IGRT, either with kV-kV match or Cone Beam CT, both of which are clinical standard.

2.1.2. Prediction phase The following equation describe the prediction phase of Kalman filter, which estimates the current position, based purely on the information of the motion distribution up to the last frame $(k-1)$:

$$\hat{\mathbf{x}}_{k|k-1} = \mathbf{F}\hat{\mathbf{x}}_{k-1|k-1} \tag{7}$$

In addition, following Kalman (1960) the current measurement error matrix $\mathbf{P}_k$ can also be estimated based on the previous distribution $\mathbf{P}_{k-1|k-1}$ and the expected distribution of prostate motion $\mathbf{Q}_k$, as described above.

$$\mathbf{P}_{k|k-1} = \mathbf{F}\mathbf{P}_{k-1|k-1}\mathbf{F}^T + \mathbf{Q}_k \tag{8}$$

2.1.3. Update phase With measurement information, $\mathbf{z}_k$, the error between the predicted and actual measurement is calculated as:

$$\widetilde{\mathbf{y}}_k = \mathbf{z}_k - \mathbf{H}_k\hat{\mathbf{x}}_{k|k-1} \tag{9}$$

with $\mathbf{H}_k$ updated based on equation (2).

The following operations are then used to calculate the optimal Kalman gain ($\mathbf{K}_k$) given the residual error of the prediction (Kalman 1960):

$$\mathbf{S}_k = \mathbf{R}_k + \mathbf{H}_k \mathbf{P}_{k|k-1} \mathbf{H}_k^T \tag{10}$$

$$\mathbf{K}_k = \mathbf{P}_{k|k-1} \mathbf{H}_k^T \mathbf{S}_k^{-1} \tag{11}$$

We can then re-estimate the current position given the current projection information:

$$\hat{\mathbf{x}}_{k|k} = \hat{\mathbf{x}}_{k|k-1} + \mathbf{K}_k \widetilde{\mathbf{y}}_k \tag{12}$$

Finally, the *a posteriori* covariance can be estimated optimally to be used for future prediction and update, as:

$$\mathbf{P}_{k|k} = (\mathbf{I} - \mathbf{K}_k \mathbf{H}_k) \mathbf{P}_{k|k-1} \tag{13}$$

2.1.4. Measurement noise matrix update To acquire 2D measurement $\mathbf{z}_k$ of the target at the current projection k, some type of segmentation of the target on the projection would be required. For prostate, this is mostly likely segmentation of the implanted fiducial markers. Most segmentation algorithms in this space to date use template matching (Flelidius et al. 2012). Thus, the measurement noise matrix can be estimated from the normalised cross correlation value, ρ_k, between the segmented marker and the template used. When there is limited information on the noise error, this value can be used as the surrogate to indicate how reliable the measurement is:

$$\mathbf{R}_k = w \begin{pmatrix} (1-\rho_k) & (1-\rho_k) \\ (1-\rho_k) & (1-\rho_k) \end{pmatrix} \tag{14}$$

the weight factor w is included as the normalised cross correlation is only a surrogate for the error. When evaluated the present method, w was set to 0.5.

With accumulated projection information, a better estimate of the measurement noise can be determined based on the recent history of measurements. For prostate motion, it is reasonable to assume that the target does not move significantly from one projection to the next. With hardware limitation of the gantry, which prevents it from moving at high speed, we can also assume that the measured target position from one frame to the next is small. Thus, the error of measurement can be estimated as:

$$\varepsilon_k = \mathbf{z}_k - \mathbf{z}_{k-1} \tag{15}$$

If N recent measurement errors are considered, the following covariance of measurement noise can be estimated:

$$\Sigma(\varepsilon_{(k-N)\to k}) = \Sigma(\varepsilon^{u_x}_{(k-N)\to k}, \varepsilon^{u_y}_{(k-N)\to k}) \tag{16}$$

Combining the equations (15) and (16), when more than N measurements are available, the measurement noise matrix can be estimated as:

$$\mathbf{R}_k = \Sigma(\varepsilon_{(k-N)\to k}) + w \begin{pmatrix} (1-\rho_k) & (1-\rho_k) \\ (1-\rho_k) & (1-\rho_k) \end{pmatrix} \tag{17}$$

Lastly, a segmentation algorithm are sometimes constrained by the pixel spacing on the detector, which is 0.388 mm in most modern linear accelerator kV systems. An additional parameter representing the error due to pixelation (0.388 mm) can be added to the overall $\mathbf{R}_k$ measurement noise matrix. For the *in silico* evaluations, $N = 10$ was used.

2.2. Evaluation framework with patients' prostate traces

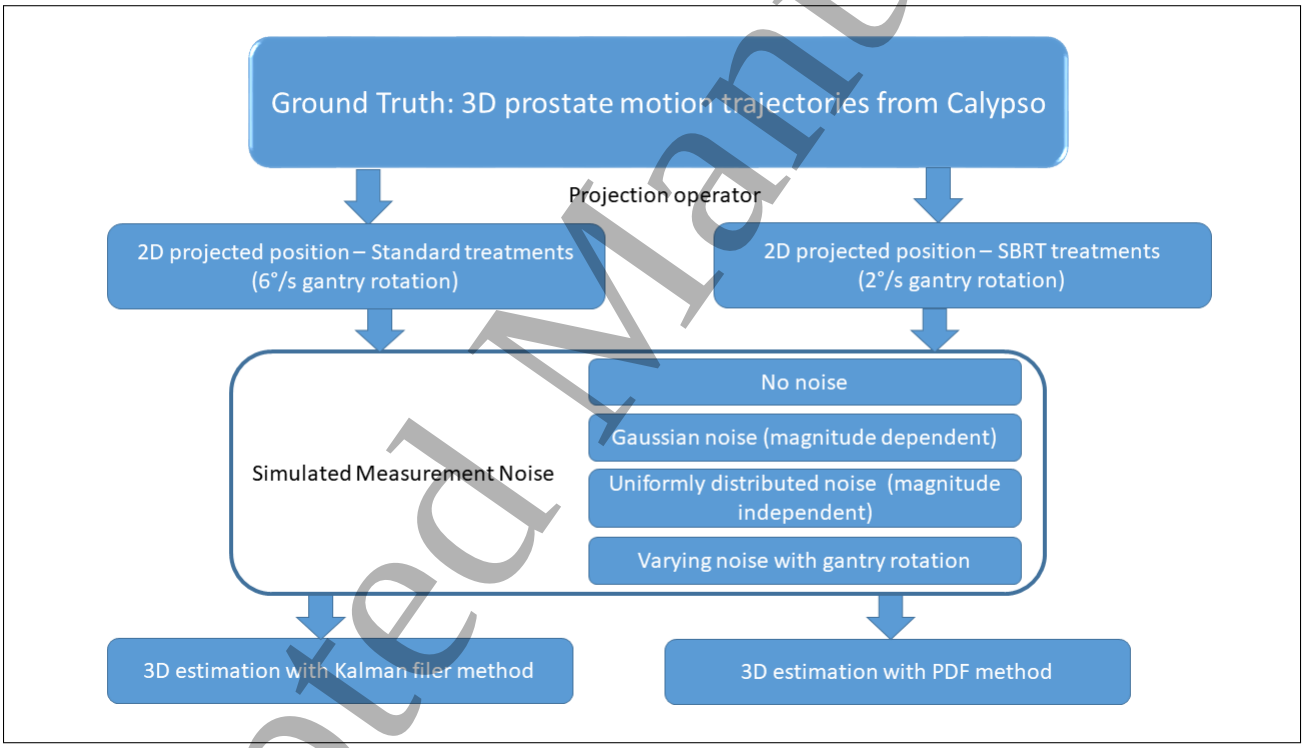

Figure 1. 3D Intrafraction prostate motion estimation using the Kalman Filter method (KF) compared with ground-truth motion and the clinically implemented PDF method. KF method is more accurate as the random-walk prostate motion is better handled. In both cases, the imaging frequency was simulated at 10 Hz with no added noise.

The evaluation framework is outlined in Figure 1. To characterise the performance and validate the Kalman method, a ground-truth dataset of 17 prostate cancer patients with implanted Calypso transponders, who were treated at the MD Anderson Cancer Centre in Orlando (FL, USA) in 2005 and 2006 Langen et al. (2008) was used. The transponders data represented the ground-truth motion of the patients' prostates during treatment, recorded at 10 Hz. Each patient had between 24 to 34 treatment fractions, each resulted in a motion trajectory in the ground-truth dataset, with length between

405 s to 800 s. In total, this ground-truth dataset consisted of 536 motion trajectories with more than 92 hours of recording. The range of motion in this database was [-3.6 4.8] mm in the x (Left-Right) direction, [-10.1 16.4] mm in the y (Superior-Inferior) direction and [-11.2 17.9] mm in the z (Anterior-Posterior) direction.

In order to test the accuracy of the proposed Kalman filter approach in estimating prostate motion, for each patient trajectory in the ground-truth dataset, the ground-truth 3D positions of the transponders were projected onto an imager using the projection equation (1). The SAD and SID value were set at 1000 mm and 1800 mm, respectively. This projection step is to simulate a realistic scenario during treatment in which radio-opaque implanted markers can be segmented from intrafraction kV images. All simulations started with the MV gantry (90° to the imaging projection angle) starts at 180°.

We investigated the accuracy and precision of the Kalman filter method at different imaging rate by down-sampling the input projection data to: 1 Hz, 0.3 z and 0.2 Hz.

The resilience of the Kalman filter method in the presence of measurement noise was also investigated. The measurement noise was modeled in two ways: (1) Gaussian white noise and (2) Random uniformly distributed noise. Both types of noise was additive noise. We also modeled pixelation for a typical pixel spacing of 0.388 mm, usually found for the X-ray imager of a linear accelerator. Gaussian white noise of two Signal-to-Noise ratios (SNRs) 5 dB and 20 dB were evaluated. For random noise, the following noise levels were tested:

- additive ± 2 *mm* random noise applied uniformly to every measurement
- additive ± 5 *mm* random noise applied uniformly to every measurement
- additive ± 5 *mm* random noise applied uniformly to measurements for gantry angles within $\pm 10°$ of the lateral imaging angles, i.e. 90° and 270°.

The last noise modeling was to simulate the effect of the reduction in imaging quality for prostate patients during treatments due to kV and MV scatter through the patient's hip bones.

For each noise scenario, we compared our method motion estimating error with the ground-truth motion. We also computed the motion estimation by the PDF method (Poulsen et al. 2009) to directly compared with our results in these scenarios.

3. Results

3.1. Theoretical accuracy

Table 1 shows the statistics of the estimating errors by the proposed Kalman filter method. The accuracy (mean error) and precision (standard deviation of error) of the proposed method are sub-millimetric in both tested gantry speed for motion in Left–Right (LR), Superior–Inferior (SI), Anterior-Posterior (AP) and 3D directions, respectively. Table 1 also includes the range of errors within 98% and 95% of the mean. An example of the prostate 3D motion estimated by KF method is shown in 2, showing

the KF method is more accurate than the PDF method in estimating the LR and AP motion.

Table 1. Accuracy and precision of the Kalman filter method in estimating patients prostate motion in the tested dataset, assuming no measurement noise. RMSE: Root Mean Square Error.

Gantry Speed	Statistics	LR(mm)	SI(mm)	AP(mm)	3D(mm)
VMAT $2°/s$	Mean ± SD	0.0 ± 0.2	0.0 ± 0.0	0.0 ± 0.3	0.2 ± 0.3
	Median	0.0	0	0	0.2
	$[2.5^{th}\ \ 97.5^{th}]$ percentile	$[-0.4\ \ 0.4]$	$[-0.0\ \ 0.0]$	$[-0.6\ \ 0.6]$	$[0.0\ \ 0.9]$
	$[1^{st}\ 99^{th}]$ percentile	$[-0.6\ \ 0.5]$	$[-0.0\ \ 0.0]$	$[-0.9\ \ 0.9]$	$[0.0\ \ 1.3]$
	RMSE	0.2	0.0	0.3	0.4
VMAT $6°/s$	Mean ± SD	0.0 ± 0.2	0.0 ± 0.0	0.0 ± 0.2	0.2 ± 0.2
	Median	0.0	0	0	0.1
	$[2.5^{th}\ \ 97.5^{th}]$ percentile	$[-0.3\ \ 0.3]$	$[-0.0\ \ 0.0]$	$[-0.4\ \ 0.4]$	$[0.0\ \ 0.7]$
	$[1^{st}\ \ 99^{th}]$ percentile	$[-0.4\ \ 0.4]$	$[-0.0\ \ 0.0]$	$[-0.7\ \ 0.6]$	$[0.0\ \ 1.0]$
	RMSE	0.2	0.0	0.2	0.3

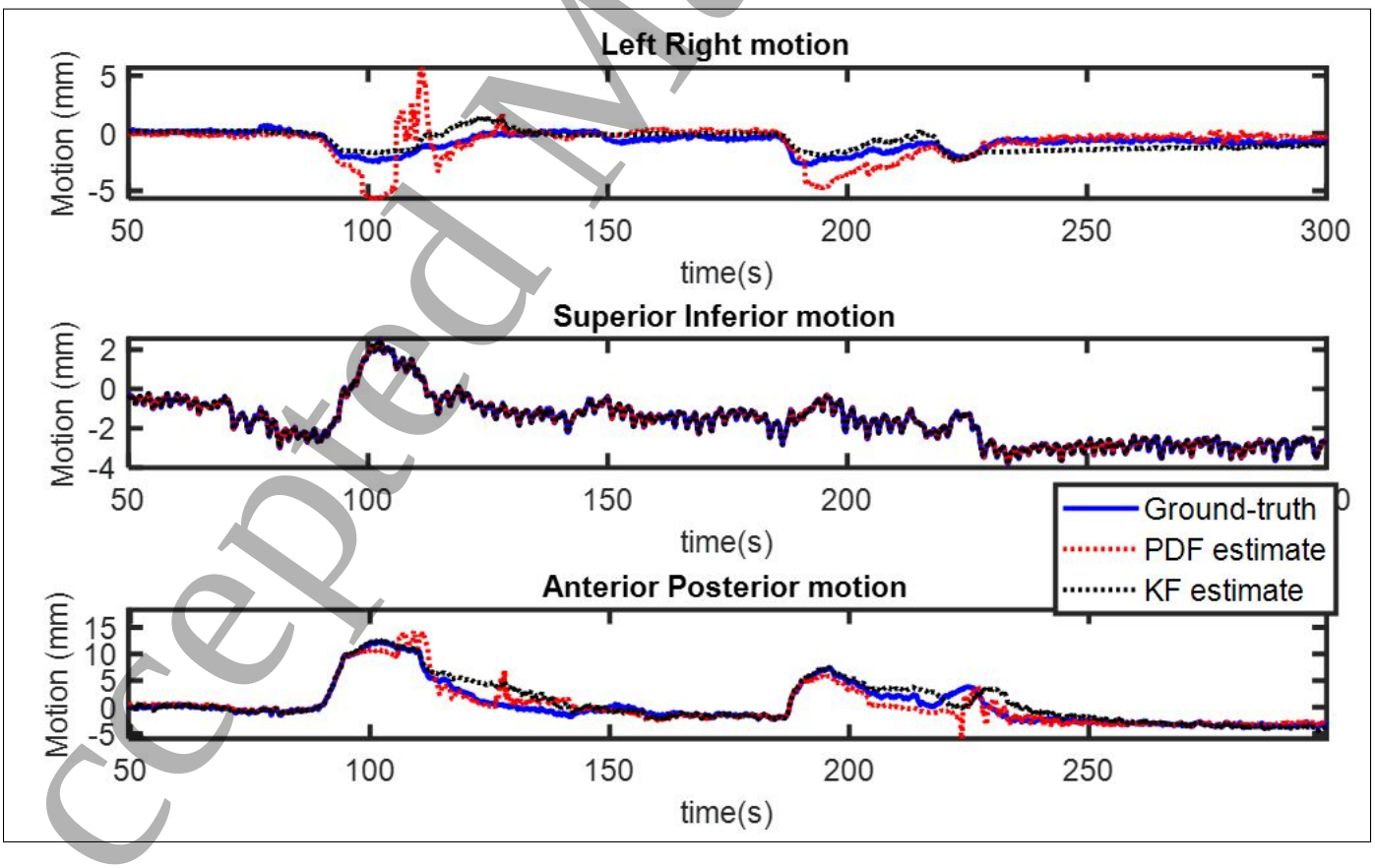

Figure 2. 3D Intrafraction prostate motion estimation using the Kalman Filter method (KF) compared with ground-truth motion and the clinically implemented PDF method. KF method is more accurate as the random-walk prostate motion is better handled. In both cases, the imaging frequency was simulated at 10 Hz with no added noise.

As the frame rate decreased, the accuracy of the Kalman filter slightly decreased, as shown in Figure 3. With imaging rates as low as 0.3 Hz, the $[1^{st} - 99^{th}]$ percentile range of errors in the LR, SI and AP directions were under 1 mm for both fast $6^{\circ}/s$ and slow $2^{\circ}/s$ gantry rotation treatments. However, with 0.2 Hz imaging rate, only the fast gantry rotation treatments had more than 98% of errors less than 1 mm. Additionally, 98% of 3D errors were less than 2 mm for all tested imaging rates.

3.2. Kalman Filter vs PDF: in the absence of measurement noise

In the absence,KFr method was as accurate and as precise as Gaussian PDF method (Poulsen et al. 2008). The 3D RMSEs for both methods, across all tested points, were 0.4 mm with slow gantry rotation and 0.3 mm with fast gantry rotation. For slow VMAT treatments, 3D errors were larger than 1 mm for 2.1% of the time when motion was estimated with Kalman filter method and for 2.5% of the time with the PDF method. With fast gantry rotation, the percentage of time with 3D errors > 1 mm decreased to 1% with Kalman filter method and 1.14% with PDF method.

For each motion trajectory in the tested dataset, the two algorithms perform similarly well. However, KF method was more consisitent in its performance with a tighter distribution of RMSE for all traces, as shown in the box plots in Figure 4.

3.3. Kalman Filter vs PDF: in the presence of measurement noise

The performance of KF method and the PDF method for each motion trajectory in the tested dataset in the presence of additive Gaussian white noise is summarised in Figure 5. With both moderate noise level (SNR=20 dB) and high noise level (SNR=5 dB), it was evident that KF method performed more consistently across more patient traces. The ranges of RMSE errors were consistently smaller with Kalman Filter method, compared with PDF method. The mean RMSE values were lower than 1 mm for LR, SI, AP and 3D errors for all tested scenarios, and were similar for both methods.

Random noise had a more profound effect on both of the algorithms, as shown in Figure 6. With additive random noise of up to ± 5 mm, across the patients motion trajectories, with PDF method, RMSEs in LR, SI, AP and 3D were all larger than 1 mm with both fast and slow gantry rotation. With KF method, the mean of RMSEs were below 1 mm for motion estimation in the LR and SI directions. On the entire dataset, with slow gantry rotation, with up to ± 5 mm random noise addition, the RMSEs were 0.5 mm, 0.9 mm, 1.2 mm and 1.5 mm in the LR, SI, AP and 3D directions, respectively, for the Kalman filter method. With the PDF method, the 3D RMSE error increased to 2.4 mm. The RMSEs were slightly lower with fast gantry rotation.

With KF method, when the measurements contained up to 5 mm random errors, 3D errors were larger 2 mm for $< 17\%$ of time while with PDF method, 3D errors were larger than 2 mm for $> 60\%$ of time. When the measurements contained up to 2 mm of random errors, the Kalman filter 3D errors exceeded 1 mm for $< 26\%$ of time, whilst the PDF 3D errors exceeded 1 mm for more than 40% of time.

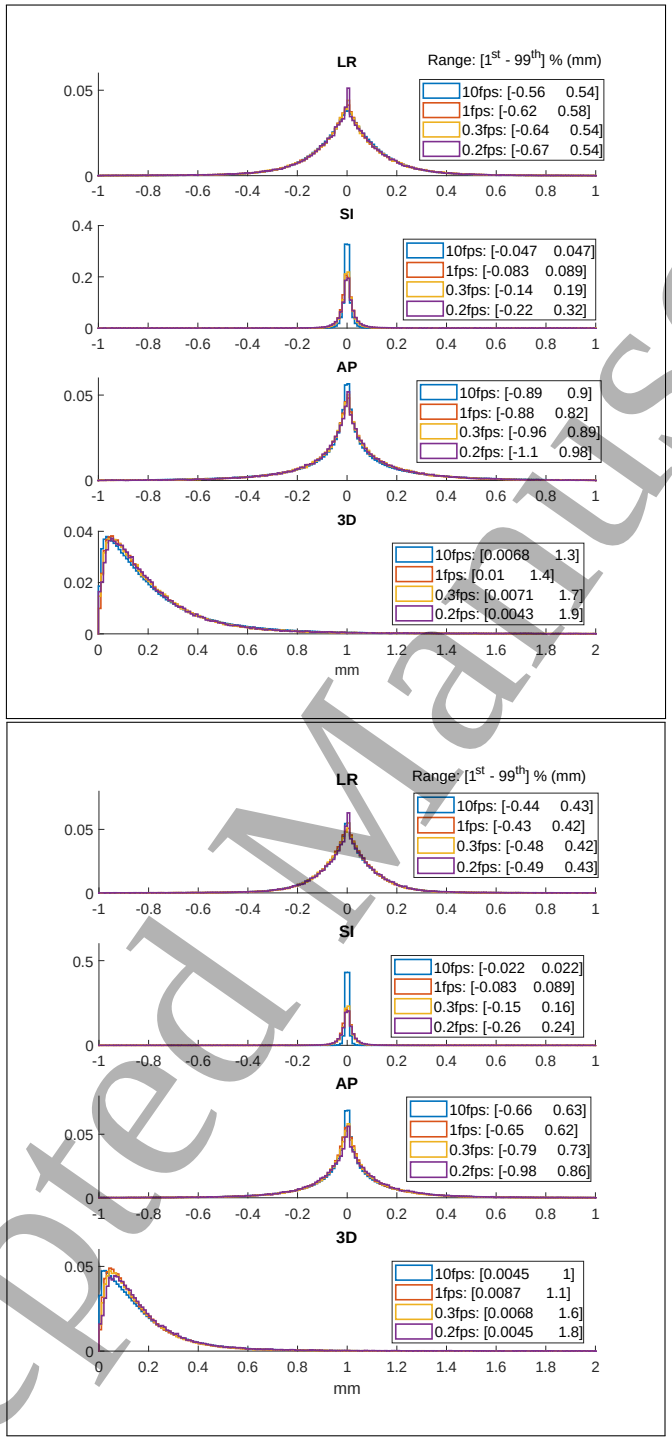

Figure 3. Histogram of motion estimation errors with the Kalman filter method with different imaging frame rates. *Above*: motion estimation error with gantry rotation speed of $2°/s$. *Below*: motion estimation error with gantry rotation speed of $6°/s$. The y–axis in each graph is the relative frequency of each bin. The bin width was set to 0.01 mm.

In the last tested scenario where the random noise only applied to measurements close to the lateral projections, as shown Figure 7, the Kalman filter performed more

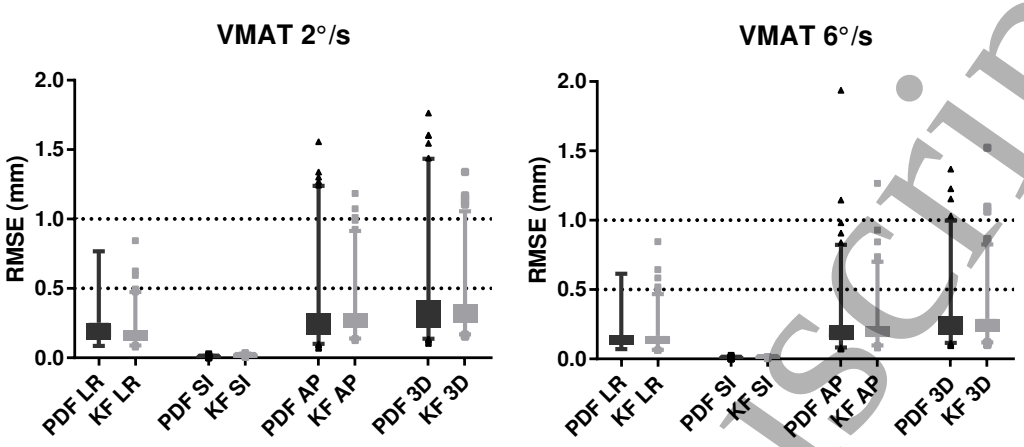

Figure 4. Box plots of the Root Mean Square Error (RMSE) in estimating patients prostate motion in the ground-truth dataset with Kalman Filter (KF) and Poulsen's et al. (2009) Gaussian PDF method (PDF), respectively. The whiskers contain 98% of data.

consistently across all 536 tested motion trajectories. Using the PDF method to estimate motion with fast gantry rotation, the 3D RMSE of 54 motion trajectories (10%) were larger than 1 mm, with 19 of these cases had 3D RMSEs larger than 2 mm. Using the Kalman filter method under the same condition, only 4 cases (0.75%) had 3D RMSE larger than 1 mm and none were larger than 2 mm.

4. Discussion

A novel method to estimate the 3D prostate tumour position during radiotherapy based on the iterative Kalman Filter algorithm was developed. A distinct advantage of this method compared to previously proposed methods (Poulsen et al. 2008) is that it does not require a learning arc to initialise. Our method was extensively evaluated in silico using a 3D prostate motion database from 17 cancer patients in two different radiotherapy treatment scenarios: normal fractionation VMAT ($6°/s$) and SBRT VMAT ($2°/s$). The database includes 536 motion trajectories, each contains 405 seconds to 800 seconds of intrafraction motion recording. The accuracy and precision of the proposed method was found to be comparable with the PDF method and was under 1 mm for all axes of motion at all tested imaging frequency. The accuracy of our method in tracking the prostate is similar to that of the electromagnetic transponder system Calypso (Santanam et al. 2008) and outperforms the reported accuracy of the commercial ultrasound guidance system Clarity (Robinson et al. 2012).

Our KF method does not require an initial learning period to initialise its parameters. Instead, a population covariance was used as the state-transition covariance (eqn.5). As the prostate is tracked on more incoming kV images, the a posteriori

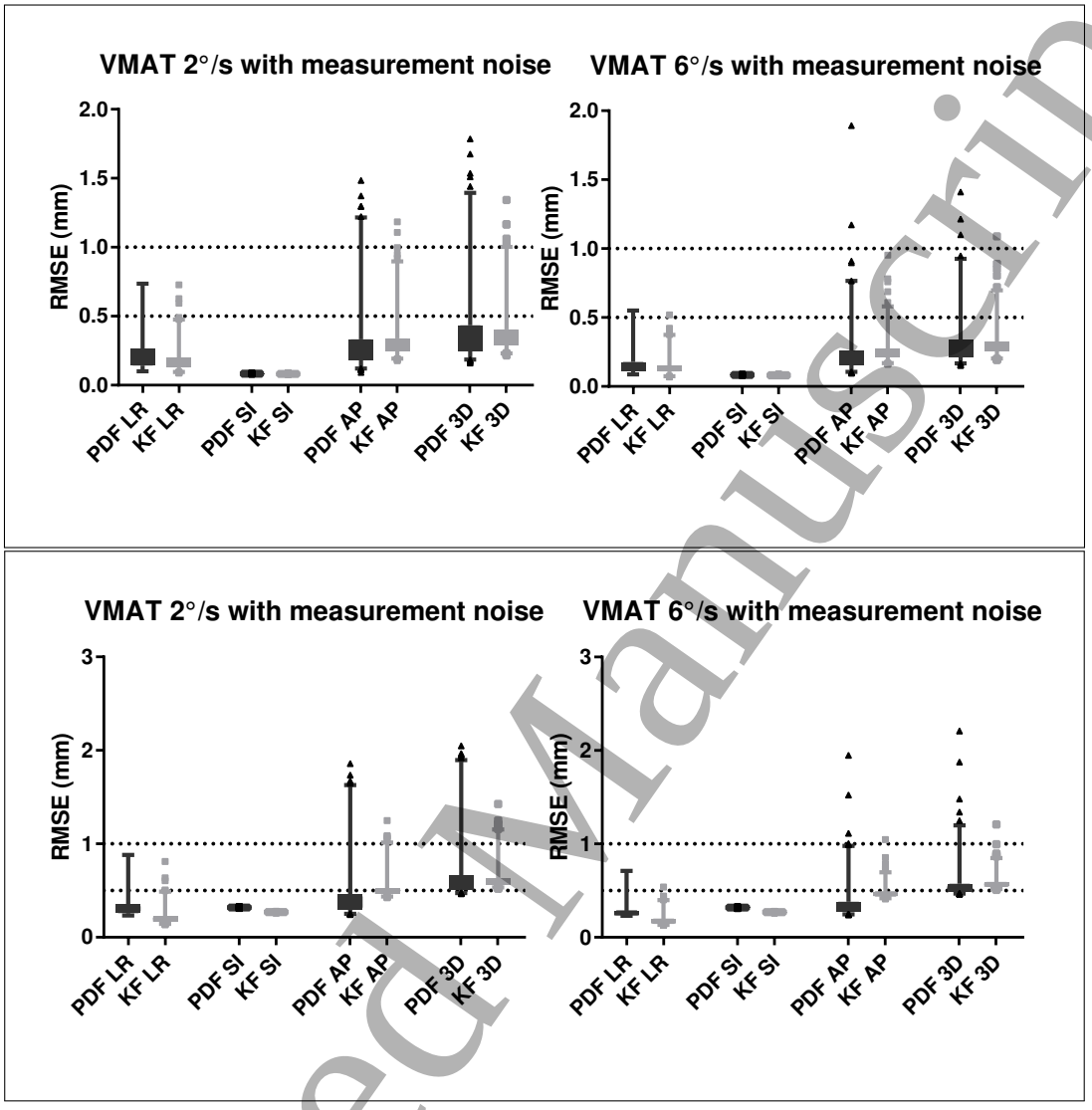

Figure 5. Box plots of the Root Mean Square Error (RMSE) in estimating patients prostate motion in the ground-truth dataset with Kalman Filter (KF) and Poulsen's et al. (2009) Gaussian PDF method (PDF) with additive Gaussian white noise, respectively. The whiskers contain 98% of data. *Top*: with SNR = 20 dB. *Bottom*: with SNR=5 dB.

covariance of the process distribution iteratively evolves to include errors from previous estimation using Eqn.8. Poulsen et al. (2009) evaluated the use of the population covariance to initialise the PDF method for prostate cancer monitoring from kV images. However, with the PDF method, the use of the population covariance resulted is less accurate result (Poulsen et al. 2009). With the proposed KF method, we were able to achieve similar accuracy and precision to the PDF method with 600 frames of initialisation. This is because the present KF method updates the motion covariance with every frame based on the last observed position of the target on the previous kV image.

Our method is more computationally efficient in that it does not require constant

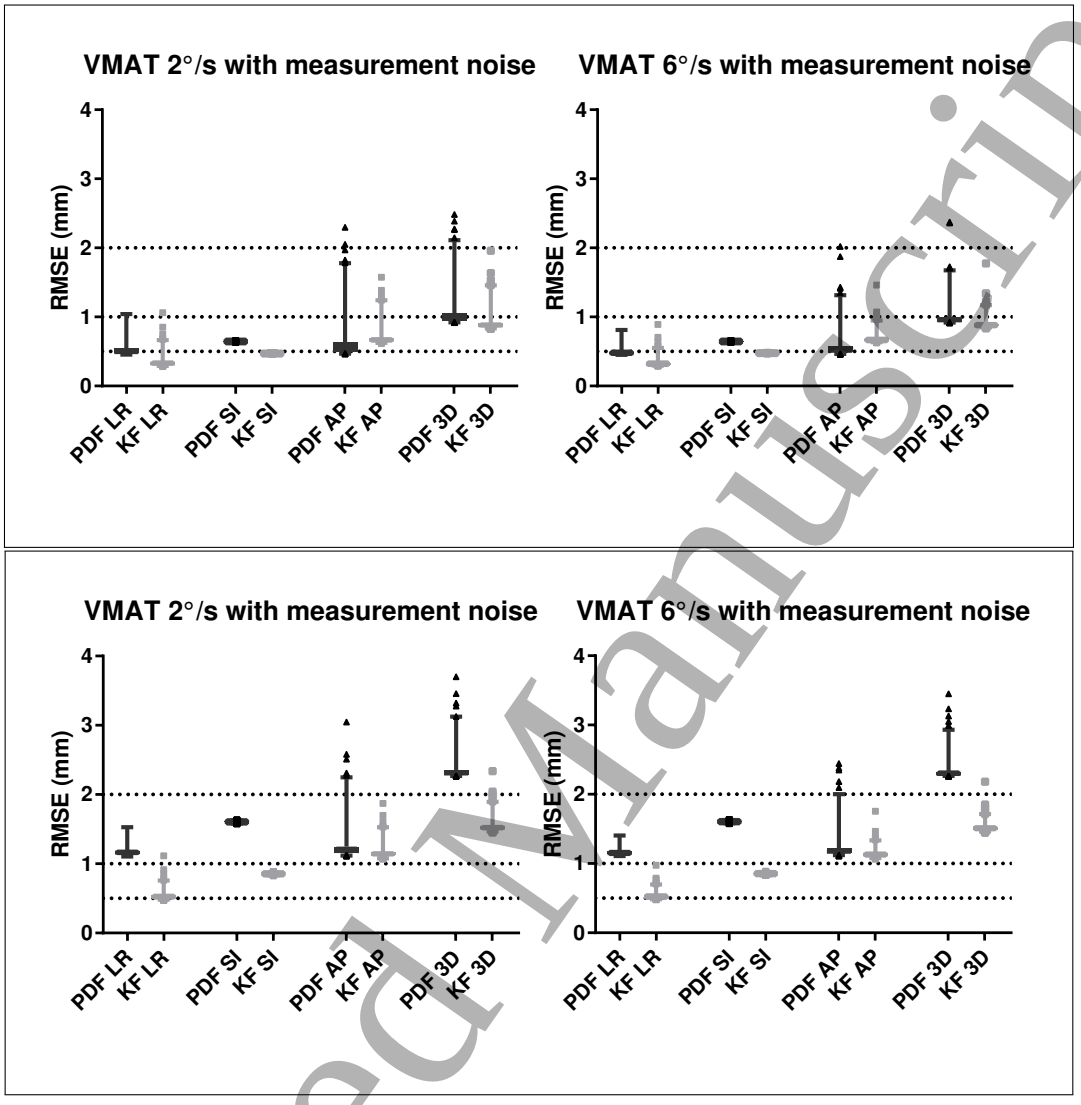

Figure 6. Box plots of the Root Mean Square Error (RMSE) in estimating patients prostate motion in the ground-truth dataset with Kalman Filter (KF) and Poulsen's et al. (2009) Gaussian PDF method (PDF) with additive randomn noise, respectively. The whiskers contain 98% of data. *Top*: with ± 2 *mm* of random noise. *Bottom*: with ± 5 *mm* of random noise.

re-optimization to handle the random-walk nature of prostate motion (Ballhausen et al. 2015). Existing methods require constant re-optimisation of parameters to handle the randomness of prostate motion (Poulsen et al. 2008, Keall et al. 2015), which is computationally expensive. Our method handles the randomness of prostate motion through the Kalman gain parameter (Eqn. 12). This process evolves iteratively with each acquired kV image, requiring no re-optimisation of parameters. In the present work, we also showed that the KF method is robust with lowering kV imaging frequency. For prostate cancer monitoring, as the target movement is typically slow, high target monitoring accuracy at lower frame rate results in less imaging dose to the patient whilst maintaining the treatment accuracy.

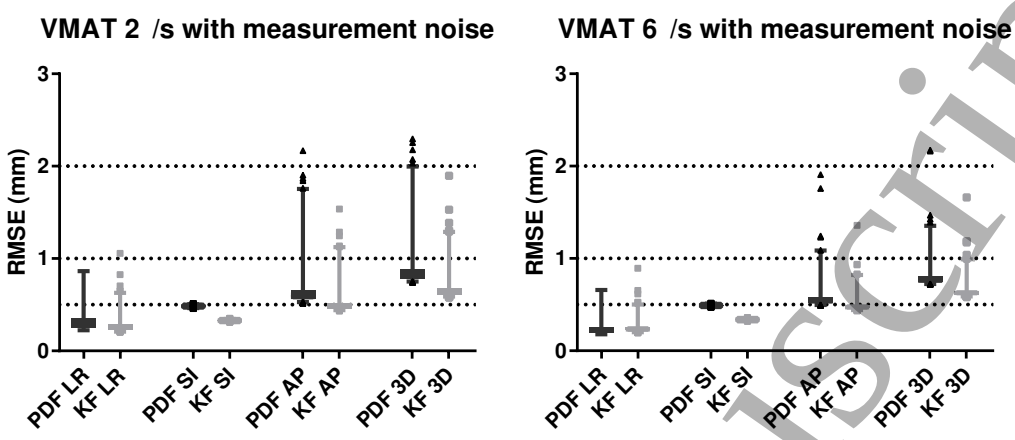

Figure 7. Box plots of the Root Mean Square Error (RMSE) in estimating patients prostate motion in the ground-truth dataset with Kalman Filter (KF) and Poulsen's et al. (2009) Gaussian PDF method (PDF) with ± 5 *mm* additive random noise at lateral imaging angles, respectively. The whiskers contain 98% of data.

Measurement noise, i.e. possible errors from marker segmentations and imaging noise, is handled explicitly with our method with Eqn.14. We evaluated the robustness of both the proposed KF method and the PDF method by increasing the measurement noise as Gaussing noise (Figure 5), random noise (Figure 6) and increasing random noise at lateral imaging angles (Figure 7). In all scenarios, especially with gantry-varying noise, the KF method was more robust than the PDF method. A limitation of this work is that noise was simulated instead of measured. A number of noise models were included to address this limitation. These include Gaussian white noise, which is dependent on the signal amplitude, random uniformly distributed noise, which is not amplitude dependent, and gantry-dependent noise. Among these noise, following an analysis of 46 prostate patient SBRT treatments reported by (Hewson et al. 2019), the gantry-dependent noise dominated other type of measurement noise during treatment due to the presence the pelvic bones in patients. The present study found that the KF method outperformed the PDF method for this type of noise. In reality, measurement noise on 2D projection is due to (1) a limitation of the segmentation algorithm and (2) a combination of kV and MV scatter collected by the kilovoltage imager. Because of first factor, the performance of KF method and its robustness against real measured noise will depend on the segmentation algorithm used to detect the targets on kV images. Given KF method interent ability to adapt to measurement noise, it is possible to achieve accurate 3D estimation with less accurate segmentation methods. Scatter noise on intrafraction kV images resembles Gaussian noise simulated in the present study as the overall noise profile is a combination of multiple random processes. All in all, it is reasonable to expect that KF method will perform better than PDF method against measurement noise in patients' images through the results of this study.

In this study, we purposefully used the Calypso database such that the ground-truth is known at all time to thoroughly evaluate the theoretically achievable performance of the KF method. In the immediate next step, we will implement and evaluate the KF method retrospectively on patients' intrafraction fluoroscopic images using an existing database such as the TROG 15.01 SPARK trial (Keall et al. 2017). For this step, the KF method will need to be combined with an appropriate segmentation algorithm to delineate the implanted fiducials. The measurement noise in such future study will directly correlate with the accuracy of the segmentation algorithm.

5. Conclusion

An iterative Kalman Filter method was developed to address the need for estimating randomly moving targets during cancer radiotherapy on a standard equipped linear accerator. Extensive evaluation of this method using different treatment scenarios shows sub-mm accuracy and precision. In addition, the present work allows the target to be monitored without the need of a learning arc, reducing additional imaging dose to the patient. Our method is also shown to be more robust against imaging and segmentation noise than the existing method.

References

Ballhausen, H., Li, M., Hegemann, N.-S., Ganswindt, U. & Belka, C. (2015), 'Intra-fraction motion of the prostate is a random walk', *Phys Med Biol* **60**(2).

Castellanos, E., Ericsson, M. H., Sorcini, B., Green, U., Nilsson, S. & Lennernäs, B. (2012), 'Raypilot – electromagnetic real-time positioning in radiotherapy of prostate cancer – initial clinical results', *Radiother Oncol* **103**(suppl 1), S433.

Cho, B., Poulsen, P. R., Ruan, D., Sawant, A. & Keall, P. J. (2012), 'Experimental investigation of a general real-time 3d target localization method using sequential kv imaging combined with respiratory monitoring', *Phys Med Biol* **57**, 7395–7407.

Chung, H., Poulsen, P. R., Keall, P. J., Cho, S. & Cho, B. (2016), 'Reconstruction of implanted marker trajectories from cone-beam ct projection images using interdimensional correlation modeling', *Med Phys* **43**(8), 4643–4654.

Fallone, B. G., Murray, B., Rathee, S., Stanescu, T., Steciw, S., Vidakovic, S., Blosser, E. & Tymofichuk, D. (2009), 'First mr images obtained during megavoltage photon irradiation from a prototype integrated linac-mr system', *Med Phys* **36**, 2084–2088.

Hewson, E. A., Nguyen, D. T., O'Brien, R., Kim, J., Montanaro, T., Moodie, T., Greer, P. B., Hardcastle, N., Eade, T., Kneebone, A., Hruby, G., Hayden, A. J., Turner, Sandra amd Siva, S., Tai, K., Hunter, P., Sams, J., Poulsen, P. R., Booth, J. T., Martin, J. T. & Keall, P. J. (2019), volume = 46, number = 11, pages = 4125–4737, type = Journal Article,), 'The accuracy and precision of the kim motion monitoring system used in the multi-institutional trog 15.01 stereotactic prostate ablative radiotherapy with kim (spark) trial', *Medical Physics* .

Kalman, R. E. (1960), 'A new approach to linear filtering and prediction problems', *Transactions of the ASME–Journal of Basic Engineering* **82**(Series D), 35–45.

Keall, P. J., Ng, J. A., Juneja, P., O'Brien, R. T., Huang, C.-Y., Colvill, E., Caillet, V., Simpson, E., Poulsen, P. R., Kneebone, A., Eade, T. & Booth, J. T. (2016), 'Real-time 3d image guidance using a standard linac: Measured motion, accuracy, and precision of the first prospective clinical trial of kilovoltage intrafraction monitoring guided gating for prostate cancer radiation therapy', *Int J Radiat Oncol Biol Phys* **94**(5), 1015–1021.

Keall, P. J., Ng, J. A., O'Brien, R., Colvill, E., Huang, C.-Y., Poulsen, P. R., Fledelius, W., Juneja, P., Simpson, E., Bell, L., Alfieri, F., Eade, T., Kneebone, A. & Booth, J. T. (2015), 'The first clinical treatment with kilovoltage intrafraction monitoring (kim): A real-time image guidance method', *Med Phys* **42**, 354–358.

Keall, P., Nguyen, D. T., O'Brien, R., Booth, J. T., Greer, P., Poulsen, P. R., Gebski, V., Kneebone, A. & Martin, J. (2017), 'Stereotactic prostate adaptive radiotherapy utilising kilovoltage intrafraction monitoring: the trog 15.01 spark trial', *BMC Cancer* **17**(180).

King, C. R., Brooks, J. D., Gill, H., Pawlicki, T., Cotrutz, C. & Presti, J. C. (2009), 'Stereotactic body radiotherapy for localized prostate cancer: Interim results of a prospective phase ii clinical trial', *Int J Radiat Oncol Biol Phys* **73**(4), 1043–1048.

Kitamura, K., Shirato, H., Shimizu, S., Shinohara, N., Harabayashi, T., Shimizu, T., Kodama, Y., Endo, H., Onimaru, R., Nishioka, S., Aoyama, H., Tsuchiya, K. & Miyasaka, K. (2002), 'Registration accuracy and possible migration of internal fiducial gold marker implanted in prostate and liver treated with real-time tumor-tracking radiation therapy (rtrt)', *Int J Radiat Oncol Biol Phys* **62**(3), 275 – 281.

Kupelian, P., Willoughby, T., Mahadevan, A., Djemil, T., Weinstein, G., Jani, S., Enke, C., Solberg, T., Flores, N., Liu, D., Beyer, D. & Levine, L. (2007), 'Multi-institutional clinical experience with the calypso system in localization and continuous, real-time monitoring of the prostate gland during external radiotherapy', *Int J Radiat Oncol Biol Phys* **67**(4), 1088–1098.

Langen, K. M., Willoughby, T. R., Meeks, S. L., Santhanam, A., Cunningham, A., Levine, L. & Kupelian, P. A. (2008), 'Observations on real-time prostate gland motion using electromagnetic tracking', *International journal of radiation oncology, biology, physics* **71**(4), 1084–1090.

Lovelock, D. M., Messineo, A. P., Cox, B. W., Kollmeier, M. A. & Zelefsky, M. J. (2014), 'Continuous monitoring and intrafraction target position correction during treatment improves target coverage for patients undergoing sbrt prostate therapy', *International Journal of Radiation Oncology Biology Physics* **91**(3), 588–594.

Nguyen, D. T., Kim, J.-H., O'Brien, R. T., Huang, C.-Y., Booth, J. T., Greer, P., Legge, K., Poulsen, P. R., Martin, J. & Keall, P. J. (2017), 'The first clinical implementation of a real-time six degree of freedom tracking system during radiation therapy', *Radiother Oncol* [**In Press**].

Poulsen, P. R., Cho, B. & Keall, P. (2008), 'A method to estimate mean position, motion magnitude, motion correlation, and trajectory of a tumor from cone-beam ct projections for image-guided radiotherapy', *Int J Radiat Oncol Biol Phys* **72**(5), 1687–1596.

Poulsen, P. R., Cho, B. & Keall, P. (2009), 'Real-time prostate trajectory estimation with a single imager in arc radiotherapy: a simulation study', *Physics in Medicine and Biology* **54**(13), 1687–1596.

Poulsen, P. R., Cho, B., Langen, K., Kupelian, P. & Keall, P. J. (2008a), 'Three-dimensional prostate position estimation with a single x-ray imager utilizing the spatial probability density', *Phys Med Biol* **53**(16), 4331–4353.

Raaymakers, B. W., Lagendijk, J. J. W., Overweg, J., Kok, J. G. M., Raaijmakers, A. J. E., Kerkhof, E. M., Put, R. W. v. d., Meijsing, I., Crijns, S. P. M. & Benedosso, F. (2009), 'Integrating a 1.5 t mri scanner with a 6 mv accelerator: proof of concept', *Phys Med Biol* **54**, N229.

Robinson, D., Liu, D., Steciw, S., Field, C., Daly, H., Saibishkumar, E. P., Fallone, G., Parliament, M. & Amanie, J. (2012), 'An evaluation of the clarity 3d ultrasound system for prostate localization', *Journal of applied clinical medical physics* **13**(4).

Santanam, L., Malinowski, K., Hubenshmidt, J., Dimmer, S., Mayse, M. L., Bradley, J., Chaudhari, A., Lechleiter, K., Goddu, S. K., Esthappan, J., Mutic, S., Low, D. A. & Parikh, P. (2008), 'Fiducial-based translational localization accuracy of electromagnetic tracking system and on-board kilovoltage imaging system', *Int J Radiat Oncol Biol Phys* **70**(3), 892–899.

Sazawa, A., Shinohara, N., Harabayashi, T., Abe, T., Shirato, H. & Nonomura, K. (2009), 'Alternative approach in the treatment of adrenal metastasis with a real-time tracking radiotherapy in patients with hormone refractory prostate cancer.', *Int J Urol.* **16**(4), 410–412.

Shimizu, S., Shirato, H., Kitamura, K., Shinohara, N., Harabayashi, T., Tsukamoto, T., Koyanagi, T. & Miyasaka, K. (2000), 'Use of an implanted marker and real-time tracking of the marker for the positioning of prostate and bladder cancers', *International Journal of Radiation Oncology, Biology, Physics* **48**(5), 1591–1597.

Shirato, H., Harada, T., Harabayashi, T., Hida, K., Endo, H., Kitamura, K., Onimaru, R., Yamazaki, K., Kurauchi, N., Shimizu, T., Shinohara, N., Matsushita, M., Dosaka-Akita, H. & Miyasaka, K. (2003), 'Feasibility of insertion/implantation of 2.0-mm-diameter gold internal fiducial markers for precise setup and real-time tumor tracking in radiotherapy.', *Int J Radiat Oncol Biol Phys* **56**(1), 240–247.

Shirato, H., Shimizu, S., Kunieda, T., Kitamura, K., van Herk, M., Kagei, K., Nishioka, T., Hashimoto, S., Fujita, K., Aoyama, H., Tsuchiya, K., Kudo, K. & Miyasaka, K. (2000), 'Physical aspects of a real-time tumor-tracking system for gated radiotherapy.', *Int J Radiat Oncol Biol Phys* **48**(4), 1187–1195.